Istituto Nazionale di Fisica Nucleare
Sezione di Pisa

INFN/AE-67/9
20 Agosto 67

$\pi^- p \to K^\circ + \Lambda^\circ(\Sigma^\circ)$ ASSOCIATED PRODUCTION BETWEEN 6 AND 11.2 GEV/C.

I.Mannelli, G.Pierazzini, A.Scribano, F.Sergiampietri M.L.Vincelli - Istituto di Fisica dell'Università di Pisa and I.N.F.N., Sezione di Pisa, Pisa, Italy.

and

C.Caverzasio, J.P.Guillaud[+], L.Holloway - Faculté des Sciences de l'Université de Paris - Institut du Radium Orsay, France.

[+] CERN Fellow.

ABSTRACT

A spark chamber experiment to measure the $\pi^- p \to K^\circ Y^\circ$ associated production at high energy has been recently completed at the CERN PS. Data has been taken at 6,8,10,11.2 GeV/c for the incident π^- momentum. We present here preliminary results at 6 and 11.2 GeV/c based on 780 and 2140 events (about 30% and 50% of the available statistics) respectively.

The sum of the $\pi^- p \to K^\circ \Lambda^\circ$ and $\pi^- p \to K^\circ \Sigma^\circ$ differential cross sections is strongly peaked in the forward direction and can be well fitted, for $|t_{min}| < |t| < 0.35$ $(GeV/c)^2$, by an exponential shape e^{at} with $a = 7.7 \pm 0.5$ $(GeV/c)^{-2}$ at 6 and $a = 7.6 \pm 0.4$ $(GeV/c)^{-2}$ at 11.2 GeV/c. The integral over the interval $|t_{min}| < |t| < 0.6$ $(GeV/c)^2$ gives 44 ± 7 μb at 6 and 20 ± 3 μb at 11.2 GeV/c, including systematic errors.

A comparison is made with previous bubble chamber results.

The experimental apparatus is shown schematically in Fig.1. The π^- beam, tipically 10^5 particles per burst, is focused on the 1.5 cm diameter, 10 cm long liquid hydrogen target(+), which is concentric with a cylindrical spark chamber containing both thin Al and Pb plates. The beam is defined electronically by four scintillation and two Cerenkov counters. Two hodoscopes, with 7×2 and 7×7 elements respectively, determine the incident π^- position with a ±.2 cm uncertainty at the target and ±.5 cm at the last spark chamber.

A picture is taken each time an incident π^- fails to give a pulse in the anticoincidence counter surrounding the target while at the same time a pulse is detected in the counter placed in front of the second spark chamber.

The hodoscope information is then BCD coded and displayed on the same film where the 90° stereo images(°) of the spark chambers are recorded. While the two thin Al foil S.C. are designed to detect the charged tracks with a minimum of multiple scattering, the last spark chamber (about 15 rad.lenghts of Pb) allows also the detection of forward emitted γ rays. We have found that in about 1 out of 10 pictures a single V type event is present, while in the majority of the others there is at least one γ ray.

The V type events selected by the scanners are measured on digitized tables. The coordinates of the sparks are reconstructed in true space with an accuracy of ±.06 cm.

(+) This special, He cooled, liquid H_2 target, designed by P.Roubeau and built at Saclay, has such geometry that it is possible to surround it with a 2.9 cm diameter anticoincidence counter, to place the last beam defining counter at only 2 cm before the liquid H_2 and to insert the whole target-counters assembly in the center of the cylindrical spark chamber, without significantly obstructing its view.

(°) No stereo is provided for the cylindrical spark chamber.

A plane is fitted through them and straight lines are fitted through the sparks which belong to the same track. The intersection of the best fit plane with the incident π^-, as defined by the two hodoscopes, is taken as the interaction point; the intersection of the two best fit lines as the neutral strange particle decay vertex. The line joining the interaction with the decay vertex is assumed to coincide with the direction of emission of the strange particle. We then calculate the partial angle θ, formed by this direction and the nearest of the two charged prongs, and the total angle θ between them. On the assumption that the observed event is indeed a $K^\circ \to \pi^+\pi^-$ decay, the K° momentum is evaluated (Fig.2) together with the invariant mass of the associated recoil and the other kinematical quantities of interest.

Events are selected on the basis of coplanarity, collinearity, opening angle, position of decay and interactions points.

The effects of the cuts introduced by the acceptance criteria have been extensively studied by comparing the experimental distributions with the Montecarlo simulated ones for various hypothesis about the production processes.

Fig.3a shows the experimental distribution at 6 GeV/c in the ratio θ/θ_{90° between the opening angle θ and the opening angle for 90° c.m. decay of a K° produced, in association with a Λ° at the observed angle of emission, by a π^-p interaction at the nominal momentum.

In Fig.3b the analogus Montecarlo generated distributions for Λ°, Σ°, Y^*_{1385} and Y^*_{1519} are shown, normalized to the values which produce the best fit linear combination to the experimental data (dotted line in Fig. 3a). As it can be seen, by requiring $0.98 \leq \theta/\theta_{90^\circ} \leq 1.10$, events with a Λ° or Σ° recoil are accepted with about equal efficiency, while only a small fraction of the events

with an isobar as recoil enter in the cut.

Another way of testing for isobar contamination, which makes use also of the information about the partial angle $\tilde{\theta}$, is provided by the distribution (for the events which satisfy the cut in θ) in the difference Δp between the K° reconstructed momentum and that one expected when the recoil is indeed a Λ°. Should a significant isobar contamination be present in the sample it would produce an asymmetry with more events with negative Δp.

By combining the two above criteria we estimate that the contamination in the samples satisfying the θ/θ_{90° cut is $\sim$ 7% at 6 and $\sim$ 15% at 11.2 GeV/c. Since in addition we have noted no systematic difference in the momentum transfer distribution for the events with positive and negative Δp, we have preferred not to introduce a cut in Δp, but simply to take into account the contamination in performing the normalization.

The empty target contribution (about 10% of the full target rate) has been subtracted bin by bin from the various distributions.

No attempt has been made, in this preliminary analysis, to evaluate the relative Λ° and Σ° production probability by looking at the γ-ray associated with the Σ° decay which, in about 25% of the cases, materialize in the Pb plates of the cylindrical spark chamber.

Fig.5 shows the resolution in the momentum transfer t for various t values at the two energies.

In Fig.6 and 7, where the differential cross sections are shown, we have also indicated the Montecarlo calculated relative detection efficiency as a function of t. The values plotted are corrected for it and the errors indicated are statistical only. The over all systematic uncertainty has been estimated to be $\pm$ 15%.

For $|t|$ smaller than 0.35 $(GeV/c)^2$ the differential cross section can be well fitted by an exponential e^{at} with $a=7.7 \pm 0.5$ $(GeV/c)^{-2}$ at 6 and $a=7.6 \pm 0.4$ $(GeV/c)^{-2}$ at 11.2 GeV/c.

Crennel et al.(Ref.3) in a bubble chamber experiment at 6 GeV/c with 448 events obtained the value $a=7.8 \pm 0.5$ $(GeV/c)^{-2}$ and a $\pi^- p \to K^\circ Y^\circ$ total cross section of 41 ± 4 μb. In Fig.8 we report $d\sigma/dt$ plots for $\pi^- p \to K^\circ \Lambda^\circ$ and $\pi^- p \to K^\circ \Sigma^\circ$ from Dahl et al.(Ref.1), between 1.9 and 4.2 GeV/c. A common feature, which persists up to our highest energy, is the marked change of slope at about $|t| = 0.4$ $(GeV/c)^2$.

No dip in the forward direction, as shown by the $\pi^- p \to \pi^\circ n$ charge exchange angular distribution, seems tc appear in our data.

We have calculated the total cross section by integrating between $|t|=|t_{min}|$ and $|t|=0.6$ $(GeV/c)^2$. The values obtained are 44 ± 7 μb at 6 and 20 ± 3 μb at 11.2 GeV/c. In Fig.7 they are shown together with previous bubble chamber results. It appears that the trend already present in the 2 to 4 GeV/c region is not in contrast with the new results at higher energy. A good fit to energy dependence can be obtained with the simple power law $E^{-3.6}$, where E is the CM total energy.

With the forthcoming data at 8 and 10 GeV/c and the improvement of statistics and reduction in systematic uncertainties at the two energies reported here, we hope it will be possible to perform a detailed theoretical analysis of this two-body strange particles production processes.

We would like to aknowledge the hospitality and support of CERN NP Division and the cooperation of the PS staff; the help received from CEN-Saclay; the collaboration of the $\pi^- p \to \overleftarrow{\pi}^\circ n$ group who runned concurrently with

us and the precious help of our technicians and scanners.

Dr.G.P.Gorini has contributed to the early stages of the experiment; Dr.M.Yvert and Mr.E.Bertolucci to the analysis.

All the calculations have been performed with the IBM 7090 of the CNUCE-Pisa.

This experiment would not have been possible without the special target built by Dr.P.Roubeau at Saclay. We like to thank him and also Mr.Derny, Dr.Borghini, Mr. Vermeulen, Mr.Uldry, Mr.Scherrer for the running of the target.

The enthusiastic support of Prof.P.Falk-Vairant and Prof.G.Stoppini throughout the experiment is gratefully aknowledged.

REFERENCES

1. O.I.Dahl, L.M.Hardy, R.J.Hess, J.Kirz, D.H.Miller, J.A. Schwartz - Preprint UCRL 17217 (January 1967).
2. R.Ehrlich, W.Selove, H.Yuta - Phys.Rev. 152,1194(1966).
3. D.J.Crennell, G.R.Kalbfleisch, K.Wu Lai, J.M.Scarr, Th. G.Schumann, I.O.Skillicorn, M.S.Webster - Phys.Rev.Lett. 18,86 (1967).
4. T.P.Wangler, A.R.Erwin, W.D.Walker - Phys.Rev.137,B414 (1965).
5. J.Bartsch, et al., Aachen,Hanburg, London, Munchen collaboration - Nuovo Cimento 43,A1010 (1966).

FIGURE CAPTIONS

Fig. 1 - Experimental apparatus. ##2,3',3,4 are the beam defining counters; hod 1 and hod 2 the two hodoscopes which determine the position of the incident π^-; #5 is the anticoincidence counter surrounding the H_2 liquid target. Two threshold gas Cerenkov counters, used for π^- and K^- selection, are not shown. SC1 and SC2 are thin Al foil spark chambers which detect the charged decay of the strange particle while the Saclay spark chamber detects also the forward γ-rays. #6, in front of SC2, is a coincidence counter.
The figure shows also the triggering logic.

Fig. 2 - $K^\circ \to \pi^+\pi^-$ kinematics at high energy. As it can be seen from the figure a measurement of the total angle θ and partial angle $\vec{\theta}$ is sufficient to determine the K° momentum. For about 85% of the available phase space the lines of constant θ and $\vec{\theta}$ are almost perpendicular to each other and, since the lines of constant θ are nearly parallel to lines of constant K° momentum, a good precision can be achieved even when $\vec{\theta}$ (as it happens in our experiment) is rather poorly known in respect to θ.

Fig.3a - Experimental distribution of θ/θ_{90° (see text).

Fig.3b - Montecarlo distribution of θ/θ_{90° (see text), for the Λ°, Σ°, $Y^*(1385)$, $Y^*(1519)$.

Fig. 4 - Momentum transfer resolution at 6 and 11.2 GeV/c for various t values.

Fig. 5 - Differential cross section $d\sigma/dt$ at 6 GeV/c and relative detection efficiency (curve down). 780 events used for the plot. The line represents χ^2-fit to the expression $d\sigma/dt = C\, e^{-at}$ in the region $|t_{min}| \leq |t| \leq 0.35$ $(GeV/c)^2$. The fitted parameters are

$a = 7.7 \pm 0.5$ $(GeV/c)^{-2}$
$C = 323 \pm 21$ $\mu b/(GeV/c)^2$
and $\chi^2 = 19$ for 15 degrees of freedom.

Fig. 6 - Idem at 11.2 GeV/c. 2140 events used for the plot.

$a = 7.6 \pm 0.4$ $(GeV/c)^{-2}$
$C = 148 \pm 8$ $\mu b/(GeV/c)^2$
$\chi^2 = 20$ for 15 degrees of freedom.

Fig. 7 - Plot of the experimentally available values for $\sigma_{tot}(\pi^- p \to K^\circ Y^\circ)$, at incident π^- momenta above 4.0 GeV/c.

Fig. 8 - Extracted from Ref.1. Differential cross sections for $\pi^- p \to K^\circ \Lambda^\circ$ between 1.9 and 4.2 GeV/c and idem for $\pi^- p \to K^\circ \Sigma^\circ$.

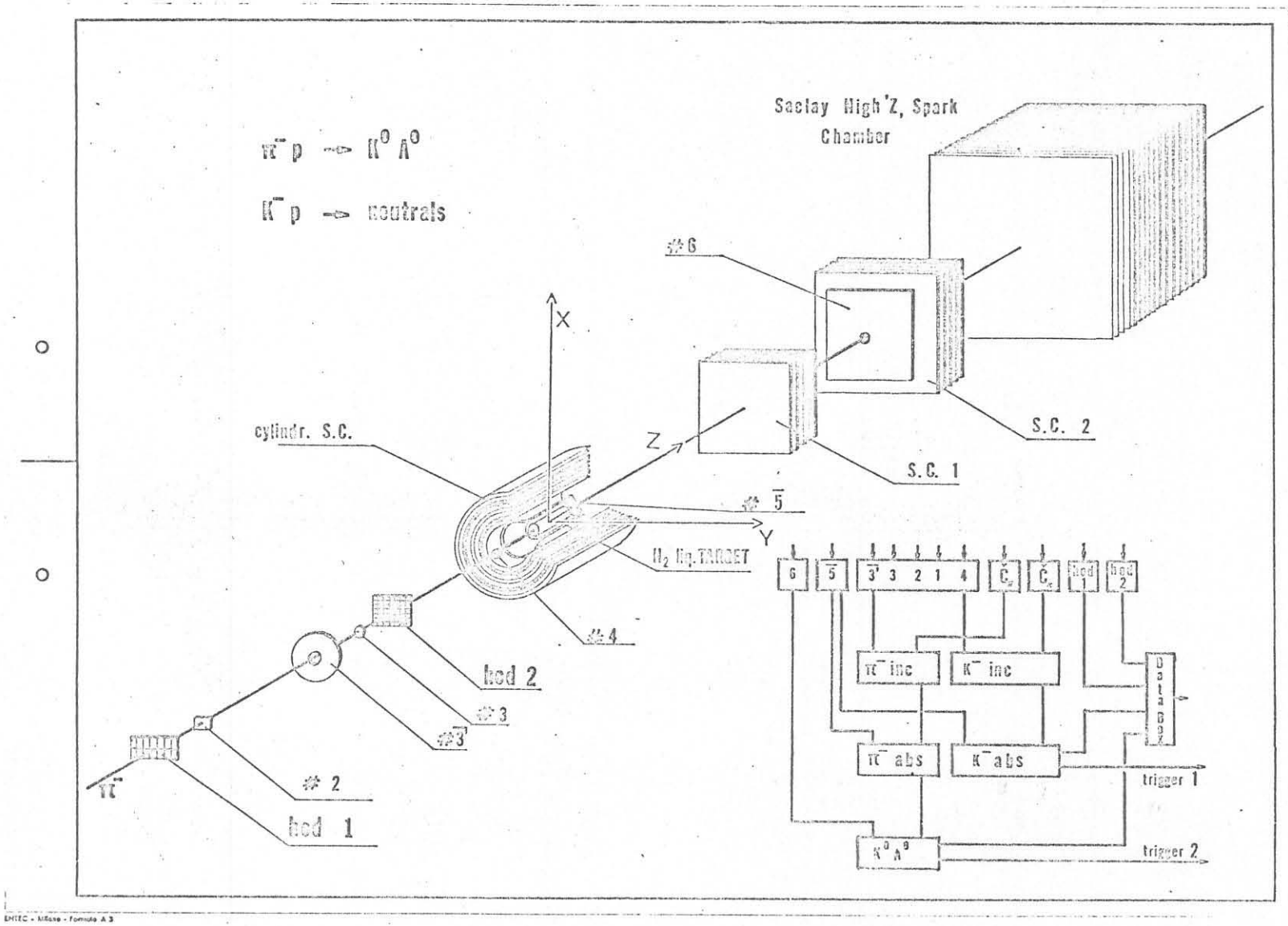
$\pi^- p \rightarrow K^0 \Lambda^0$
$K^- p \rightarrow$ neutrals
Saclay High'Z, Spark Chamber
#6
X
Z
Y
cylindr. S.C.
S.C. 2
S.C. 1
$\bar{5}$
H_2 liq. TARGET
#4
hod 2
#3
$\bar{3}$
2
hod 1
π^-
G
$\bar{5}$
$\bar{3}$ 3 2 1 4
$\bar{C}_2$
$\bar{C}_1$
hod 1
hod 2
π^- inc
K^- inc
Data Box
π^- abs
K^- abs
trigger 1
$K^0 \Lambda^0$
trigger 2

FIG. 1

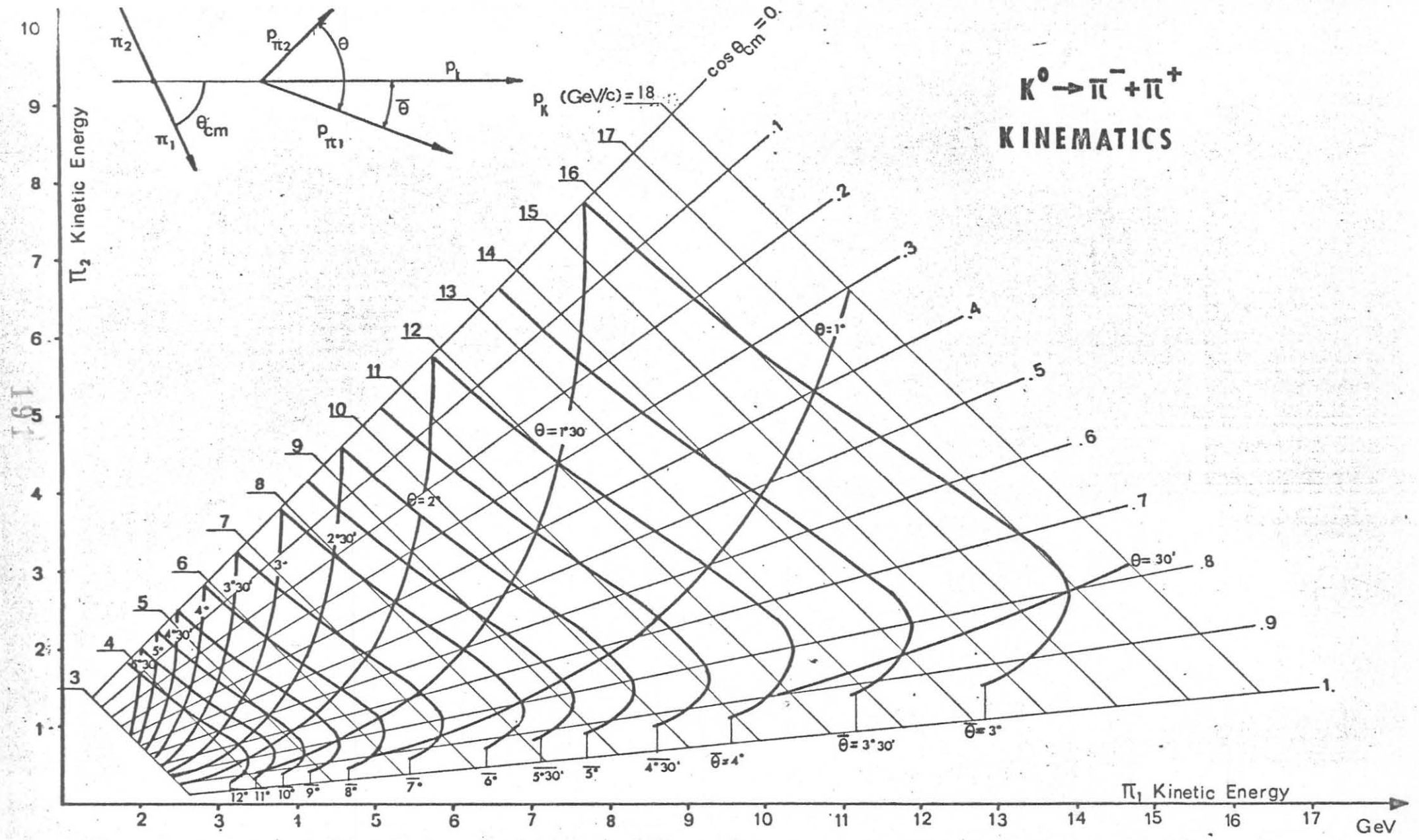
$K^0 \rightarrow \pi^- + \pi^+$
KINEMATICS
π_2 Kinetic Energy
π_1 Kinetic Energy
GeV
p_K (GeV/c) = 18
$\cos\theta_{cm} = 0.$
π_2
$p_{\pi 2}$
θ
p_1
θ_{cm}
π_1
$p_{\pi 1}$
$\bar{\theta}$
θ=1°
θ=1°30'
θ=2°
2°30'
3°
3°30'
4°
4°30'
5°
5°30'
θ= 30'
$\bar{\theta}$= 3°30'
$\bar{\theta}$= 3°
$\bar{\theta}$=4°
4°30'
5°
5°30'
6°
7°
8°
9°
10°
11°
12°

FIG. 2

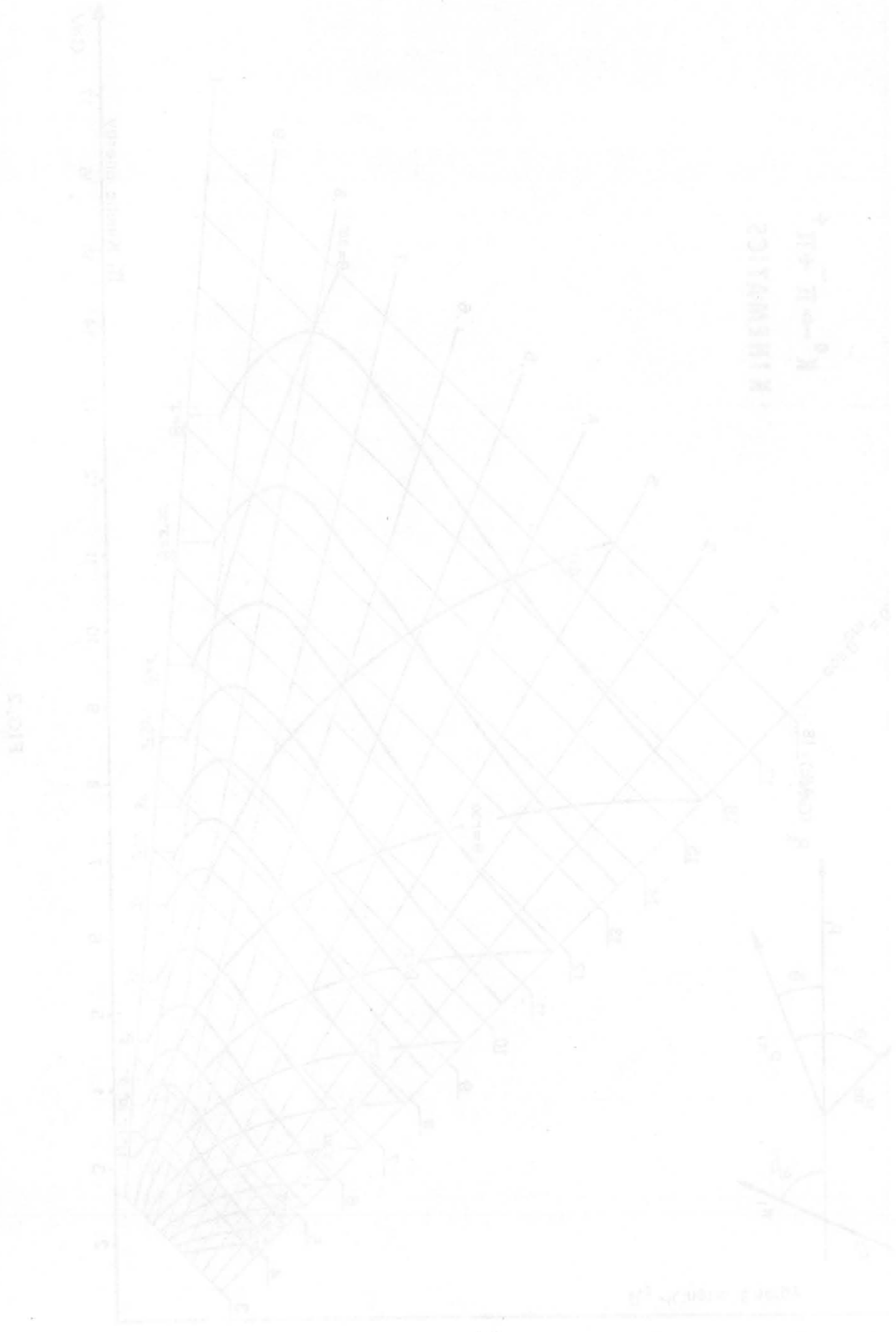

Fig. 3a

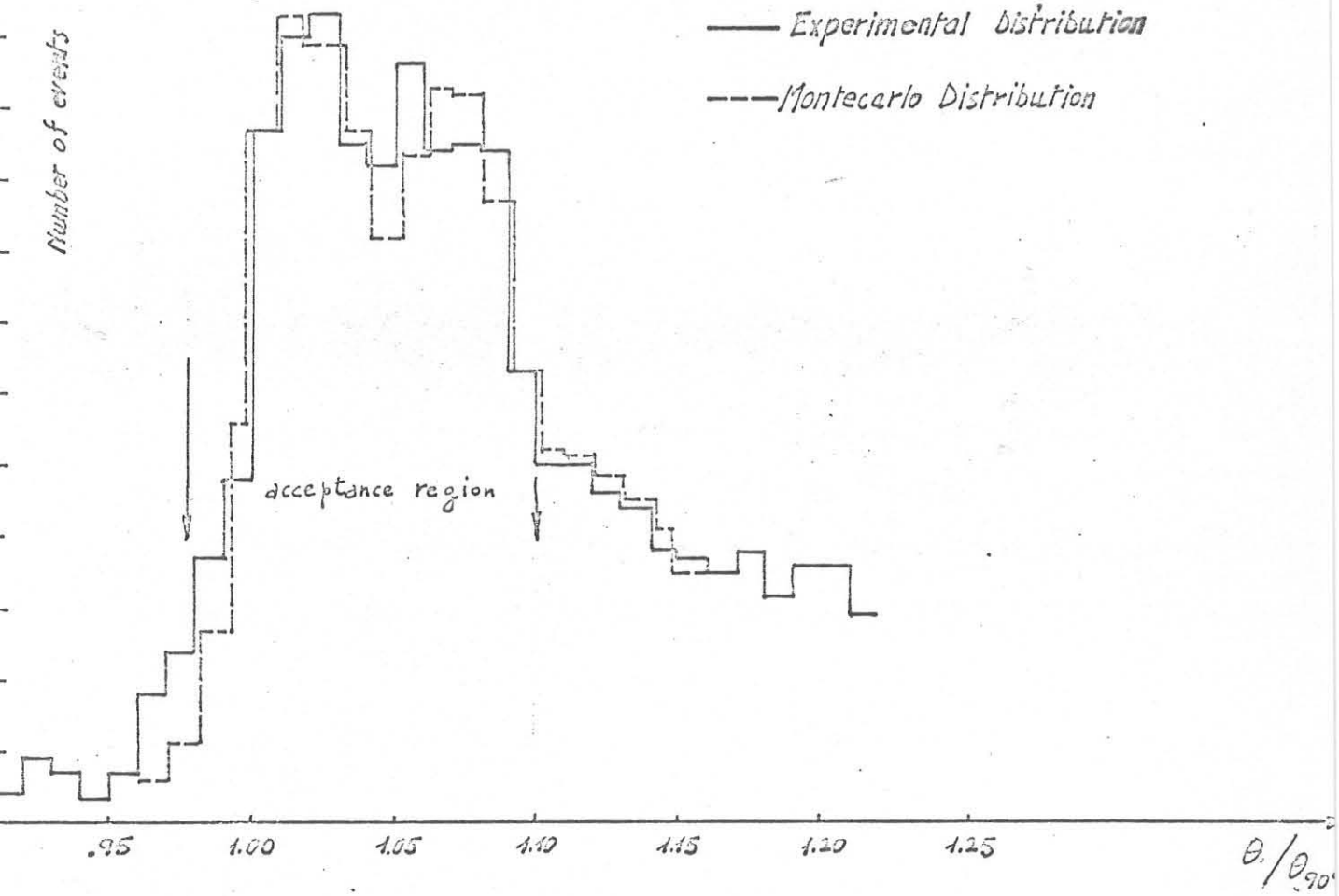
Experimental distribution
Montecarlo Distribution
Number of events
acceptance region
.95
1.00
1.05
1.10
1.15
1.20
1.25
θ/θ90°

Fig. 3b

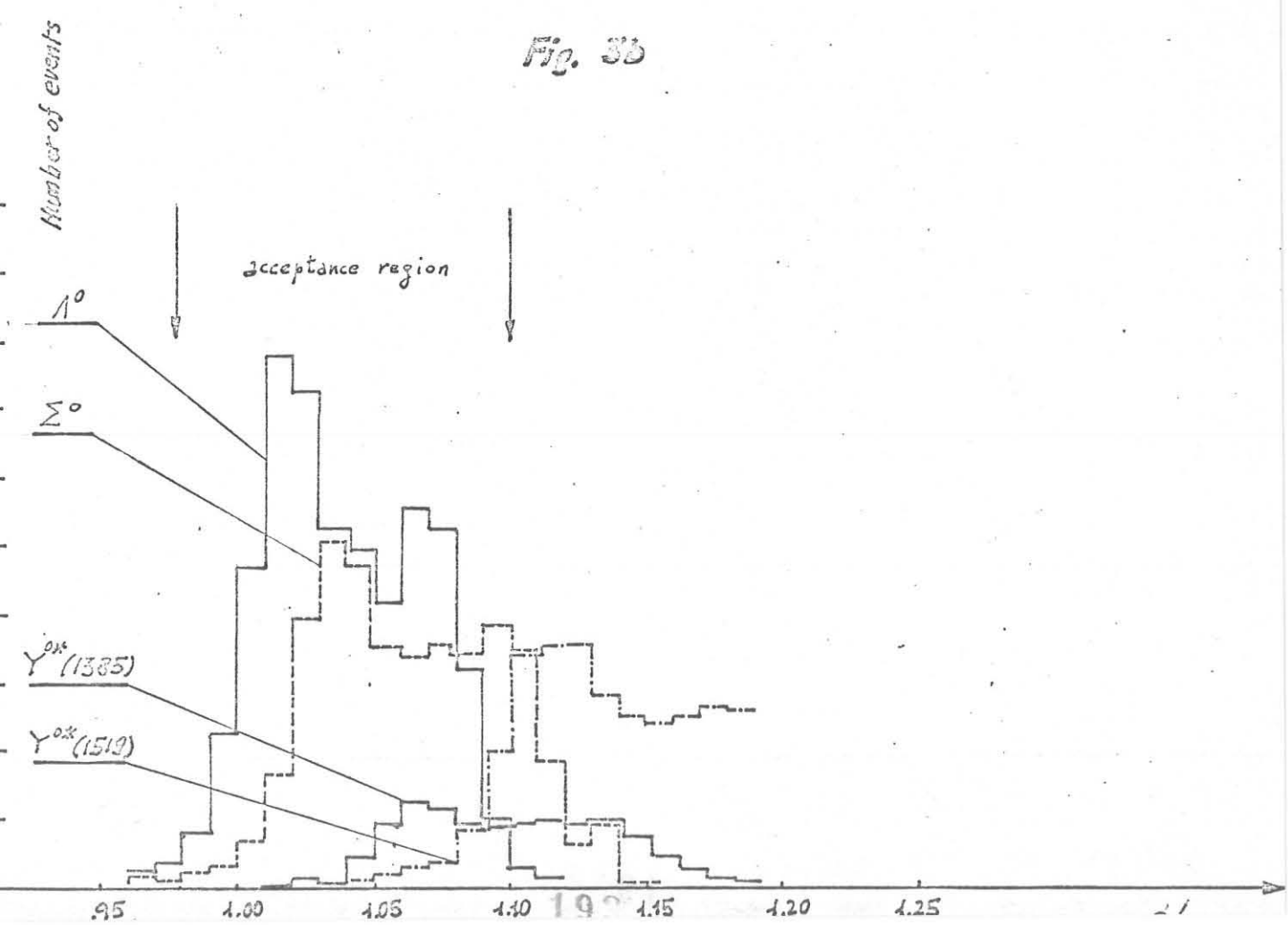
Number of events
acceptance region
Λ°
Σ°
Y°K(1385)
Y°K(1519)
.95
1.00
1.05
1.10
1.15
1.20
1.25

Momentum transfer resolution

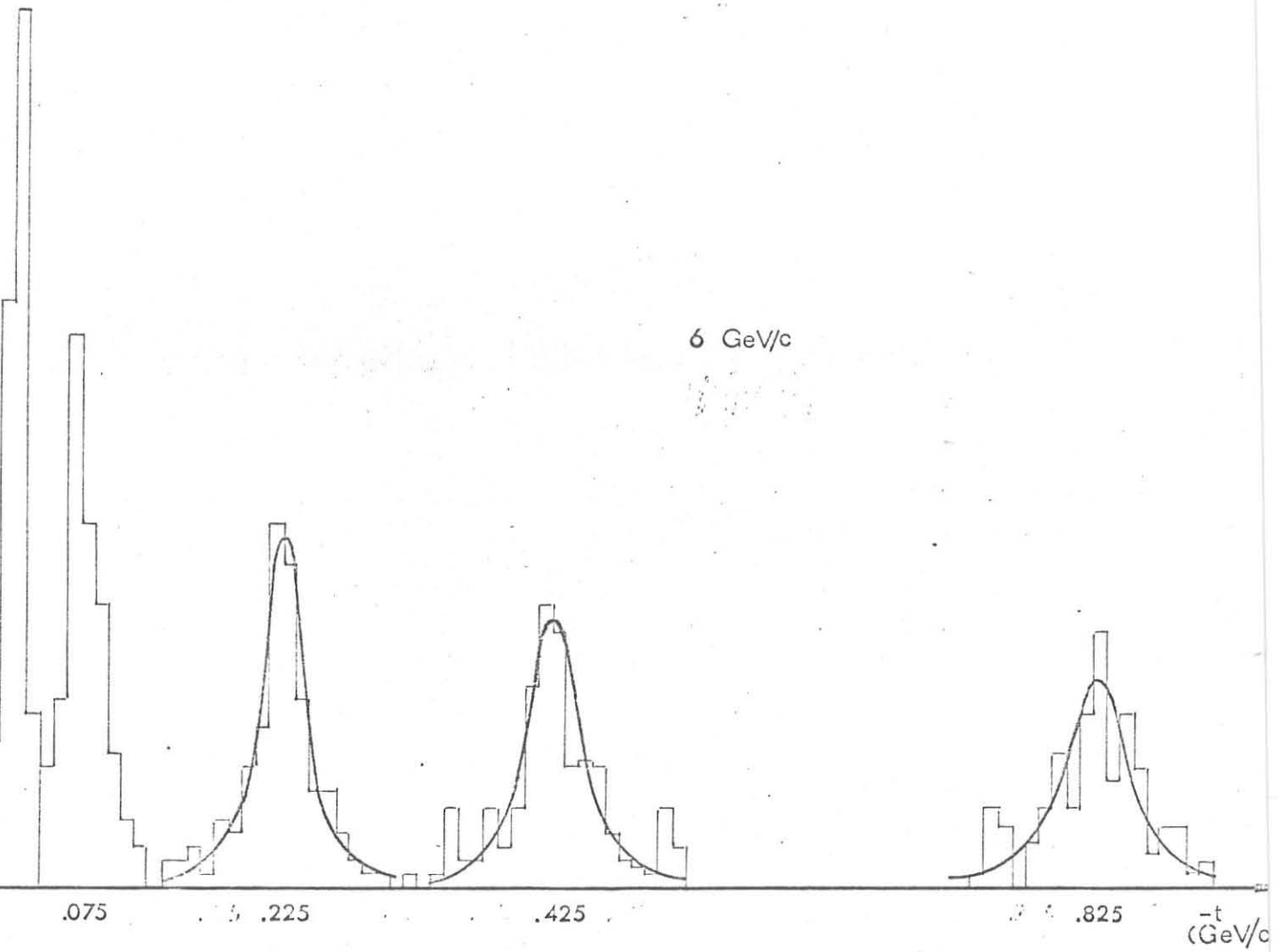

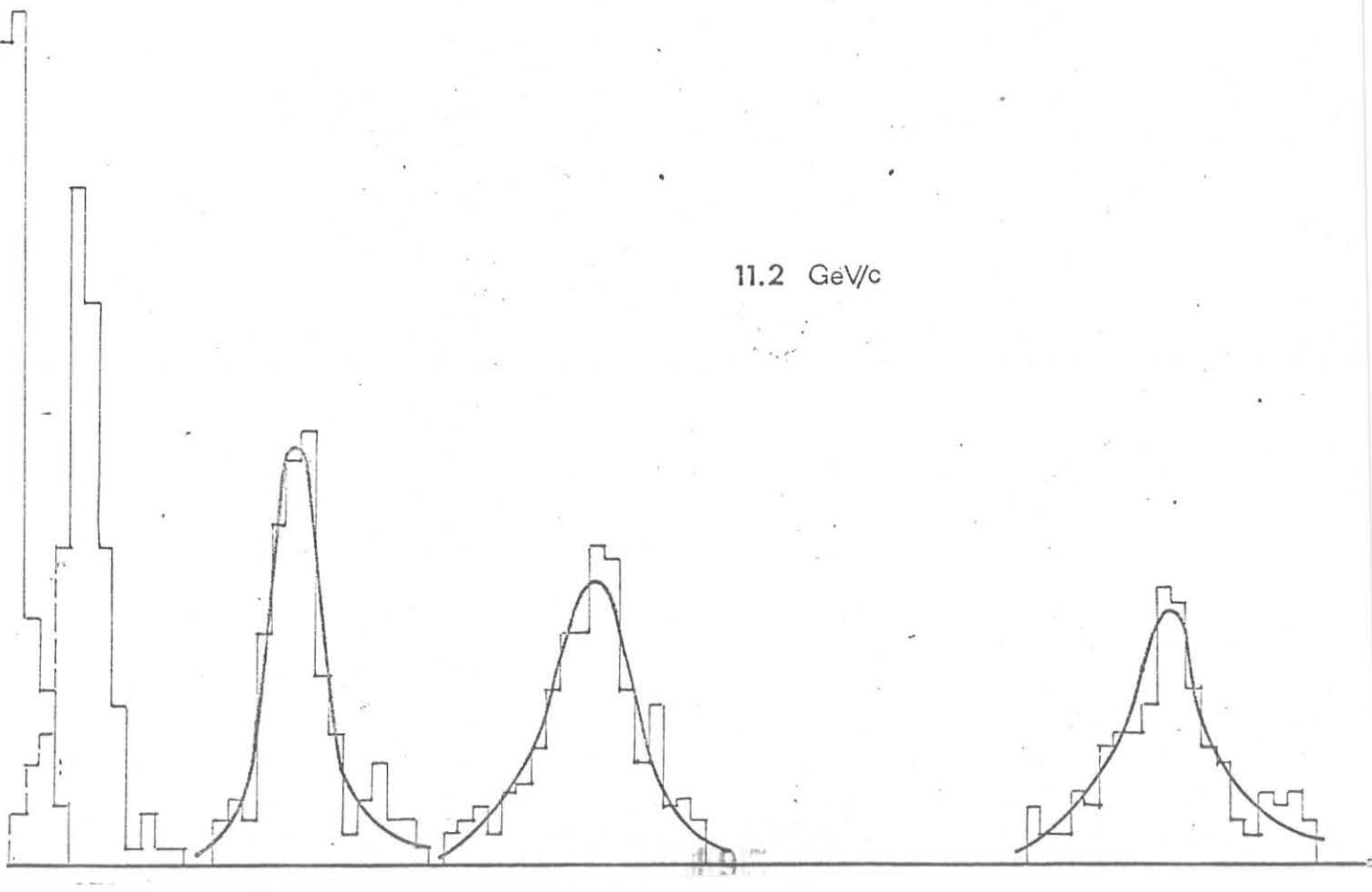

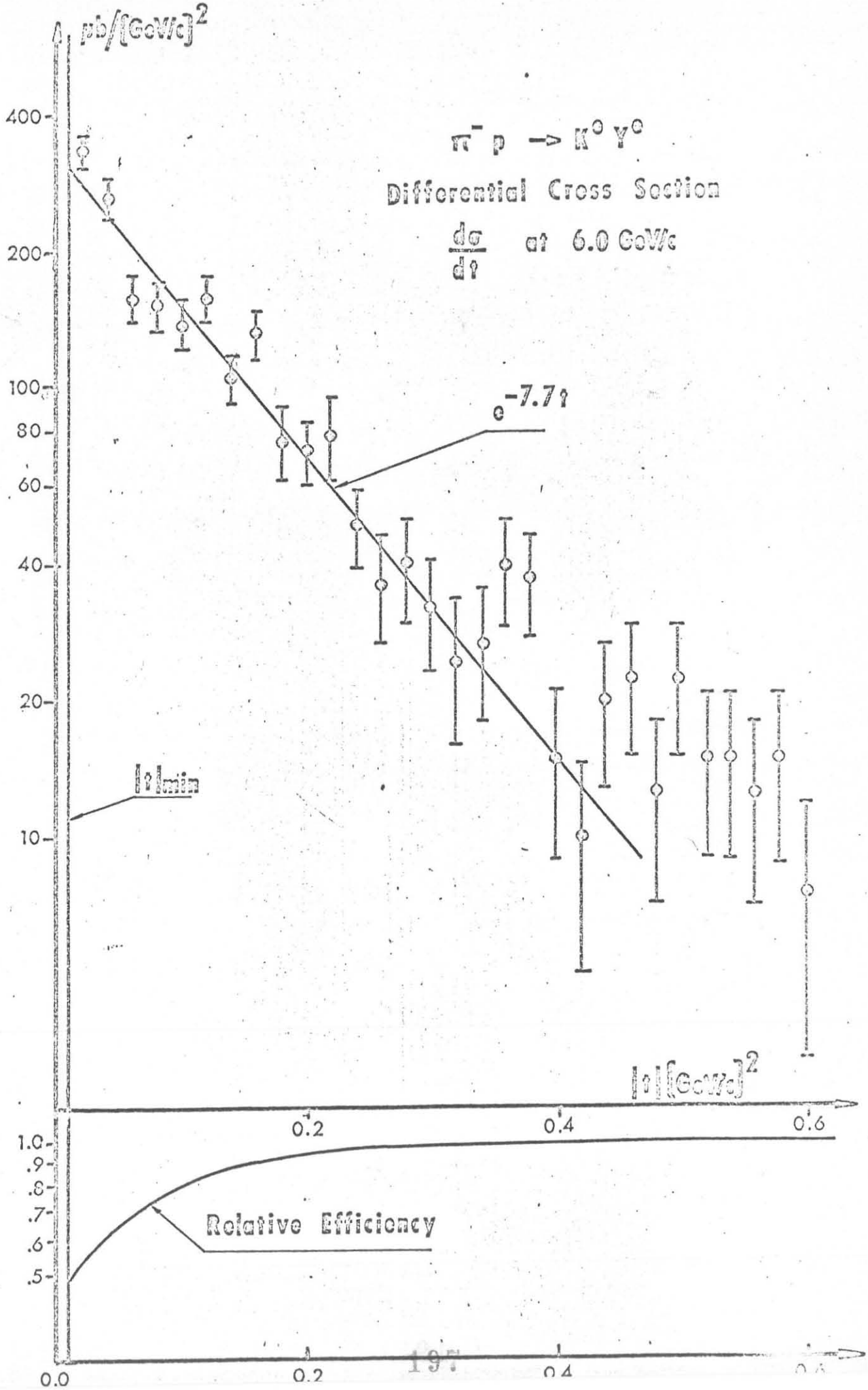
μb/[GeV/c]²
400
200
100
80
60
40
20
10
π⁻ p → K⁰ Y⁰
Differential Cross Section
dσ/dt at 6.0 GeV/c
e^-7.7t
|t|min
|t| [GeV/c]²
0.2
0.4
0.6
1.0
.9
.8
.7
.6
.5
Relative Efficiency
0.0
0.2
0.4

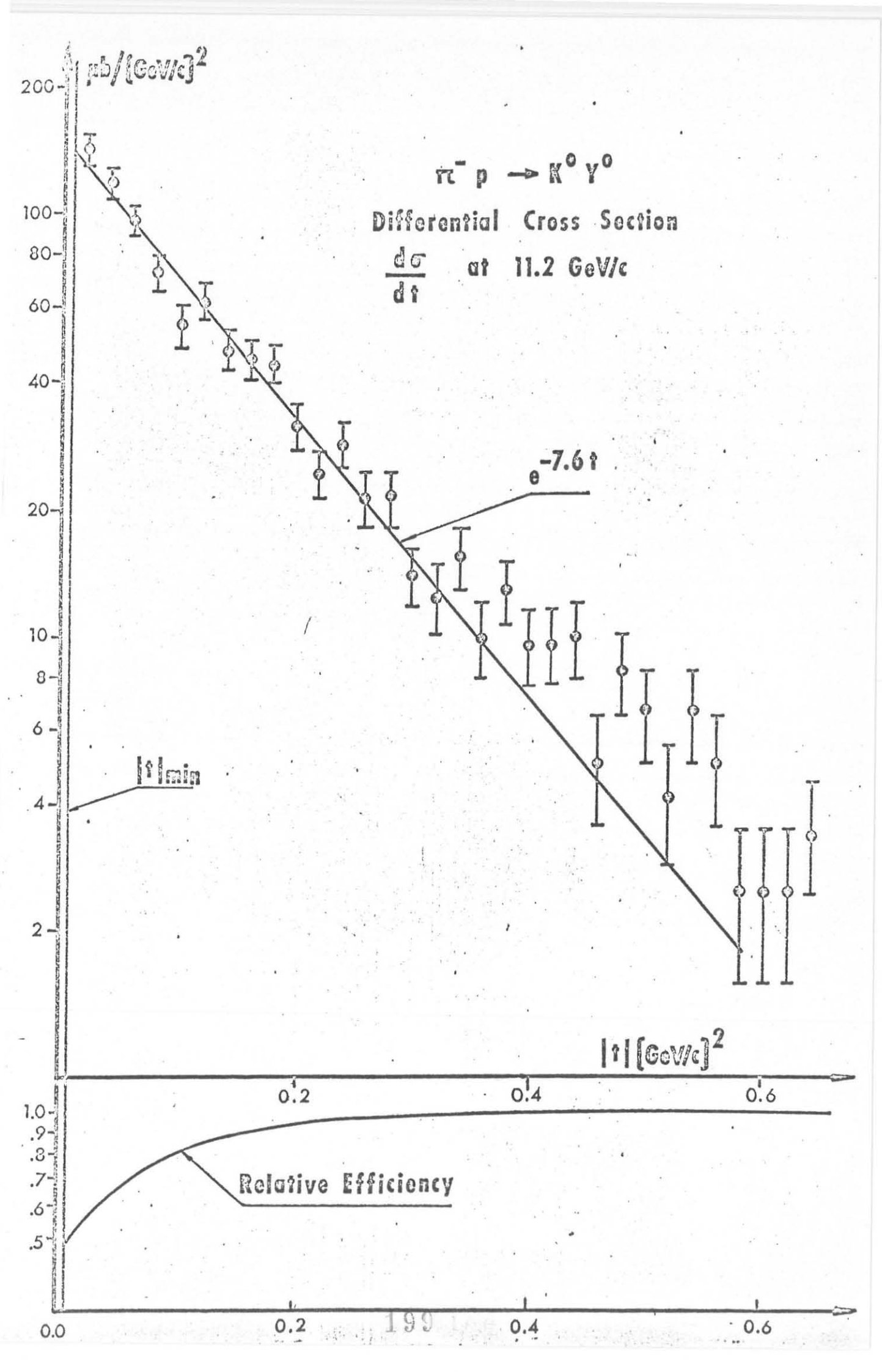
μb/[GeV/c]²
200
100
80
60
40
20
10
8
6
4
2
π⁻ p → K⁰ Y⁰
Differential Cross Section
dσ/dt at 11.2 GeV/c
e^-7.6t
|t|min
|t| [GeV/c]²
0.2
0.4
0.6
1.0
.9
.8
.7
.6
.5
Relative Efficiency
0.0
0.2
0.4
0.6

$\sigma_{tot}(\pi^- + p \rightarrow K^0 + Y^0)$

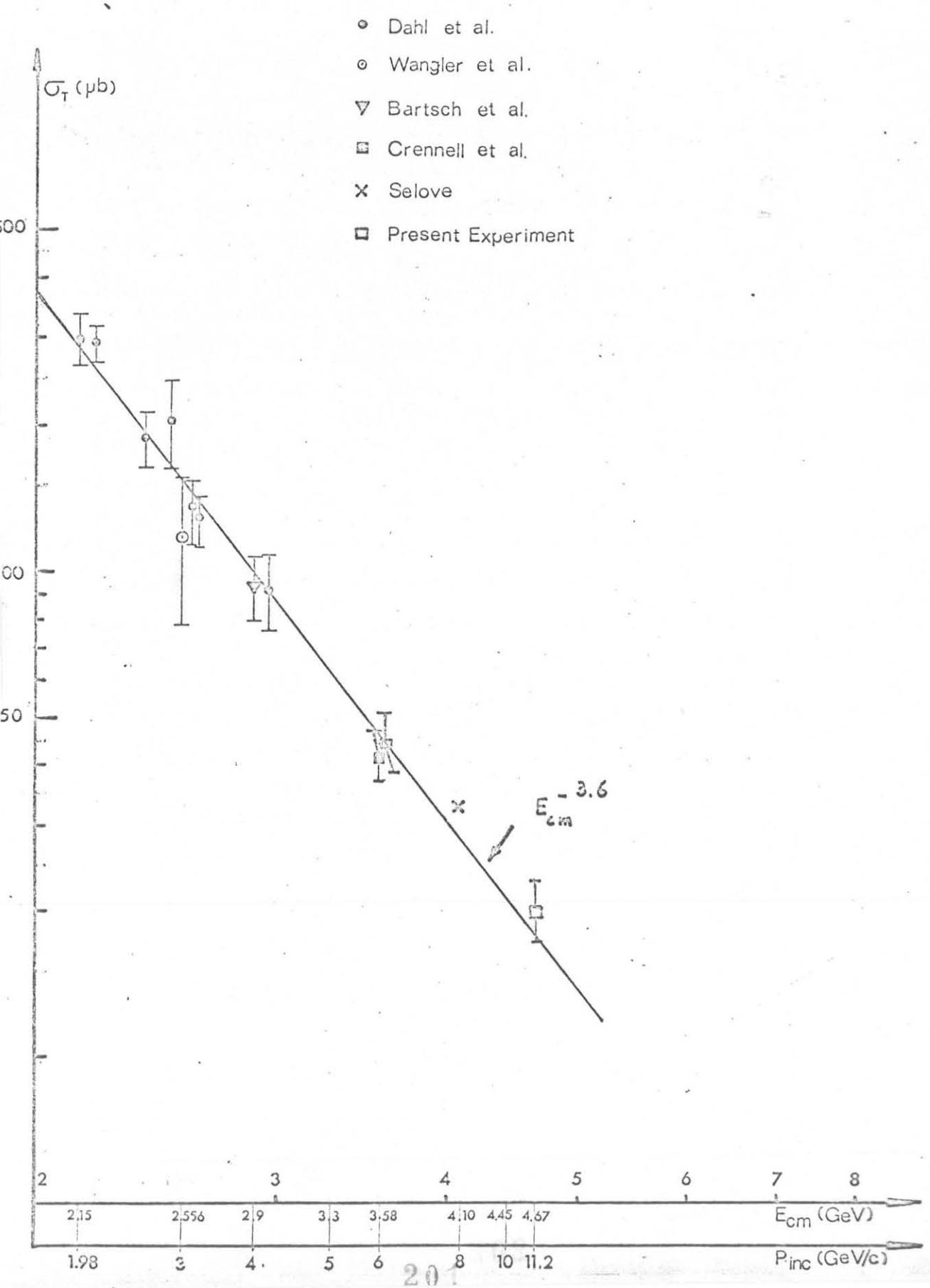

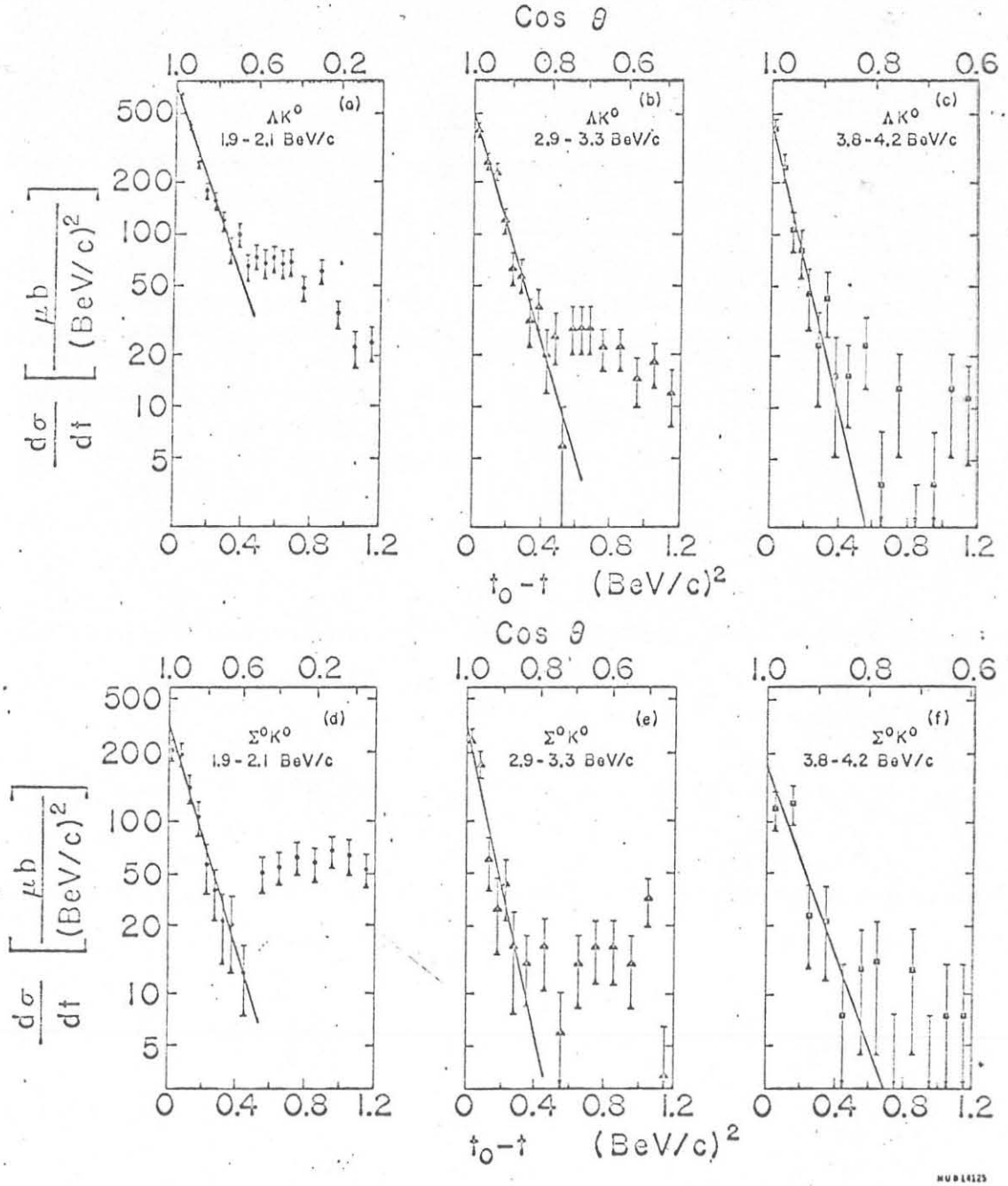
Cos θ
1.0 0.6 0.2
1.0 0.8 0.6
1.0 0.8 0.6
ΛK⁰ (a)
1.9 - 2.1 BeV/c
ΛK⁰ (b)
2.9 - 3.3 BeV/c
ΛK⁰ (c)
3.8 - 4.2 BeV/c
dσ/dt [μb/(BeV/c)²]
500
200
100
50
20
10
5
0 0.4 0.8 1.2
t0 - t (BeV/c)²
Cos θ
Σ⁰K⁰ (d)
1.9 - 2.1 BeV/c
Σ⁰K⁰ (e)
2.9 - 3.3 BeV/c
Σ⁰K⁰ (f)
3.8 - 4.2 BeV/c
MUB 14125

Fig. 8